Enhanced Electrochemical Capacitance of Graphene Nanosheets Coating With Polyaniline for Supercapacitors

Xinlu Li[*], *Hongfang Song, Yonglai Zhang, Hao Wang, Kun Du, Hongyi Li, Yuan Yuan, Jiamu Huang*

School of Materials Science and Engineering, Chongqing University, Chongqing, 400030, P. R. China
[*]E-mail: lixinlu@cqu.edu.cn

A composite of polyaniline (PANI) and graphene nanosheets (GNS) with three-dimensional (3-D) framework structure was prepared via in situ polymerization. The morphology and microstructure of the composite were characterized by scanning electron microscopy, transition electron microscopy and X-ray diffraction. Electrochemical property was examined by cyclic voltammetry and galvanostatic charge-discharge cycles. The microstructure analysis indicates that the PANI homogeneously deposits on the surface of GNS at low content but tend to aggregate between GNS at high content. The electrochemical performance show that the GNS with undestroyed framework are effective to enhance the electrochemical capacitance of the composite. A remarkable specific capacitance of 261.4 F/g (based on GNS/PANI composites with low content of PANI) is obtained at a current density of 100 mA/g compared to 190.6 F/g for pure GNS.

Keywords: graphene nanosheets, polyaniline, framework, supercapacitors

1. INTRODUCTION

Supercapacitors, as an intermediate system between dielectric capacitors and batteries have attracted a great deal of interest due to the growing demand for power systems with significant energy at high power [1]. Porous carbon materials, conducting polymers and transition-metal oxides are widely used as electrode materials for supercapacitors . Recently, graphene nanosheets (GNS), as two-dimensional layers of sp^2-bonded carbon [2], display numerous appealing features to make it a promising electrode material for supercapacitor. Compared with the conventional carbon materials, GNS show many advantages such as mass production at low cost, exceptional thermal stability, high surface area, and excellent conductivity. Graphene-based supercapacitors were reported to have a specific capacitance of 135 F/g in aqueous KOH [3] and 117 F/g in aqueous H_2SO_4 electrolyte [4].

However, the practical capacitance of GNS is far from the theoretical capacitance of 550 F/g for graphene[5]. GNS tend to irreversibly agglomerate and restack during the electrode preparation [6]. And the electrochemical capacitive of GNS is affected by the penetration of electrolyte into the restacked layers. Considerable efforts have been made to inhibit the agglomeration of GNS and improve the accessibility of electrolyte into electrode. For example, the GNS deposited with carbon black particles showed the enhanced capacitance (175.0 F/g) due to the increased space between the graphene sheets, which facilitated the diffusion of electrolyte into GNS[7]. In another way, GNS were anchored with metals [8], metal oxides[9], carbon nanotubes[10], carbon spheres[11] and conducting polymers[12, 13] to inhibit the agglomeration. Besides, much effort was done to prepare PANI/GNS to provide synergistic performances. For instance, Wang et al. reported a simple process to synthesis a nanocomposite of graphene oxide doped with PANI via in situ polymerization to improve the electrochemical capacitance performance of PANI [14]..

However, in previous work, little attention has been paid to the effect of the framework of graphene on the structure and electrochemical performance of the composites. In this paper, we prepare the composite of GNS coated with PANI by in situ polymerization. The morphology, microstructure and electrochemical performance of the GNS/PANI composite have been investigated systematicly. The work will focus on the framework of graphene and the electrochemical performance of the composite.

2. EXPERIMENTAL

2.1 Synthesis of GNS/PANI composites

All the chemicals were of analytical grade. Graphite oxide (GO) was synthesized using natural graphite (30 μm) by a modified Hummers method [15]. GNS was prepared by the exfoliation of GO by microwave irradiation as described elsewhere [16].

GNS/PANI composites were synthesized through in situ polymerization of aniline monomer in the presence of GNS suspension [17]. The mass ratio of GNS to aniline is varied as 1:1.9, 1:19 and signed as GP_1, GP_2. In a typical procedure, for GP_1, 1 mmol 1R)-(−)-10-Camphorsulfonic acid (CSA, 98%) was added into 20 mL GNS suspension (5 g/L) and the mixture was ultrasonicated for 30 min. During vigorously stirring in an ice bath, aniline (2 mmol) was rapidly poured into the above mixture and stirred for another 30 min. Then, 10 ml pre-cooled ammonium persulfate (APS, the molar ratio of aniline/APS is 1) was added to the mixture drop by drop. The reaction was kept for 20h with continuous stirring in the ice bath. Finally, the product was collected and washed repeatedly with distilled water, then dried in a vacuum oven at 80 ^{o}C for 24 h.

2.2 Microstructure Characterization

The crystallographic structure of the materials were analyzed by X-ray diffraction system (XRD, DMAX-2500PC) equipped with Cu Kα radiation (λ= 0.15406 nm). The morphology of materials were observed by transmission electron microscopy (TEM, LIBRA 200FE) and field-

emission scanning electron microscopy (FESEM, ZEISS nova 400), respectively. Brunauer–Emmett–Teller (BET) specific surface area and pore size distribution were measured by nitrogen adsorption/de-adsorption using an automatic adsorption system (ASAP 2020 M). Fourier transform infrared spectroscopy (FTIR) spectra were recorded on a GX spectrometer.

2.3 Electrode preparation and electrochemical measurement

The electrode was prepared by loading the mixture of 80 wt.% of the materials, 10 wt.% of carbon black and 10 wt.% of polyvinylidone difluoride on a nickel foam. All electrochemical measurements were done in a two electrode configuration using CR2430 coin cells [18]. The measurements were conducted in a 6 M KOH aqueous electrolyte at room temperature. These cells were charge–discharged galvanostatically on the battery tester (BTS0105C8). Cyclic voltammograms (CV) were measured by Solartron (1287+1260 8w). The galvanostatic charge/discharge and CV were performed within the voltage range of 0.0-1.0 V. For the cyclic voltammetric measurements, the sweep rate ranged from 10, 25, 50, 100 mV s^{-1} and galvanostatic charge/discharge curves were measured at different current densities of 0.1, 0.3, 0.5, 0.8 and 1 A/g.
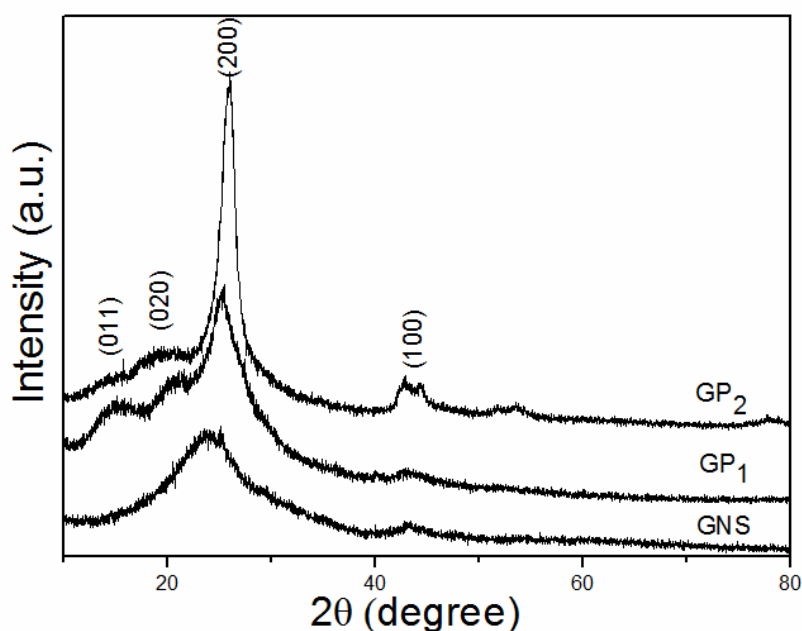
3. RESULTS AND DISCUSSION

Figure 1. XRD patterns of GNS, GP$_1$ and GP$_2$.

The XRD patterns of GNS, GP$_1$ and GP$_2$ are shown in Fig.1. In the case of GNS, the diffraction peaks at 2θ= 24.5^o and 42.8^o can be attributed to the graphite-like structure (0 0 2) and (1 0 0), respectively[19]. For GP$_1$, the diffraction peaks appears at about 2θ = 15.3^o, 20.7^o and 25.2^o, corresponding to (0 1 1), (0 2 0) and (2 0 0) crystal planes of PANI in its emeralddine salt form [20],

while the diffraction peaks at 42.8° corresponds to (1 0 0) plane of GNS. In the case of GP_2, the intensity of (2 0 0) crystal planes of PANI increases, indicating that the PANI content of the composites increases.
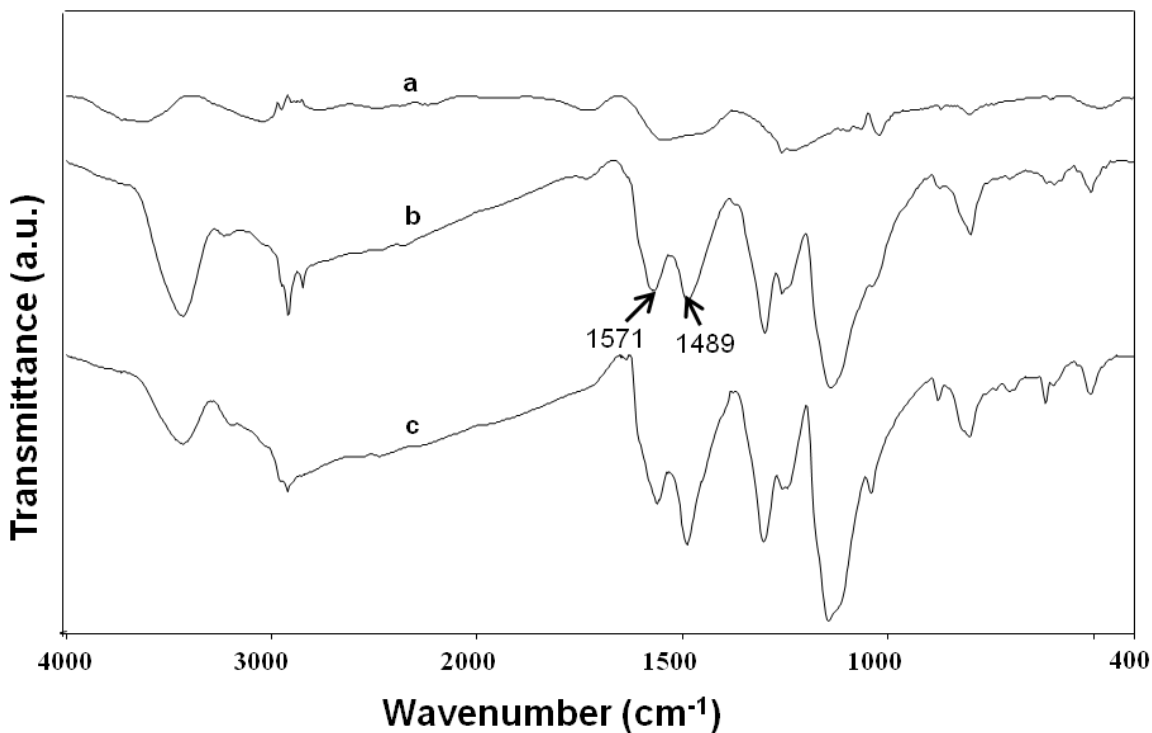

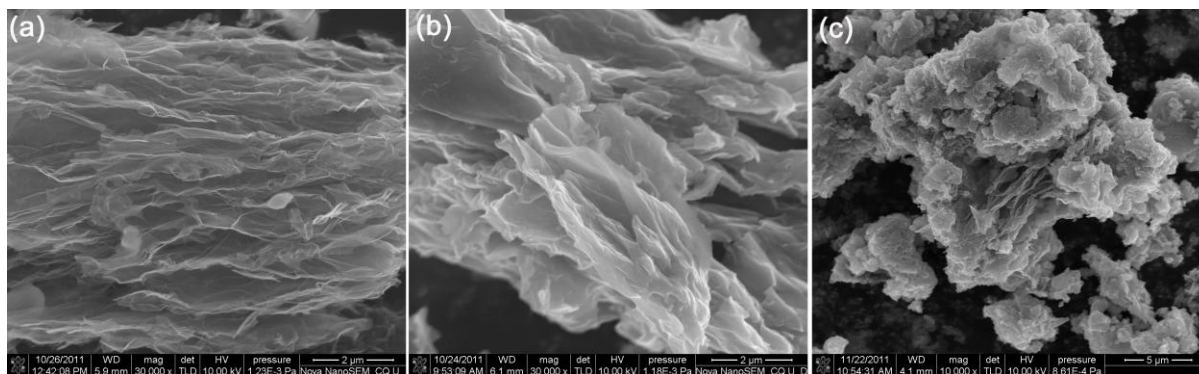**Figure 2.** FTIR spectra of (a) GNS, (b) GP_1 and (c) GP_2.

Figure 3. SEM images of (a) GNS, (b) GP_1 and (c) GP_2.

Fig. 2 shows the FTIR spectra of GNS, GP_1 and GP_2. The FTIR spectrum of GNS shown in Figure 2a indicated that the microwave-assisted reduction of GO was relatively complete with few oxygen-containing groups [21]. As shown in curves (b) and (c), the characteristic bands at 1571 and 1489 cm^{-1} (Figure 2b) were ascribed to C-C stretching deformation of quinoid and benzene rings [22], respectively, whereas the bands in the 1200-1400 cm^{-1} were related to the C−N stretching band of an

aromatic amine [23]. The presence of the above bands suggested the PANI was coated successfully on the surface of GNS.

Fig. 3 presents the morphology of GNS, GP_1 and GP_2. In Fig. 2a, it can be seen that GNS are wrinkled and folded with porous structure. As for GP_1 in Fig. 3b, PANI have been grown homogeneously on GNS' surface, resulting in three-dimensional (3-D) framework structures. In the case of GP_2, the aggregation of PANI particles is clearly observed in Fig. 3c with the destruction of the three-dimensional (3-D) framework structures. In general, the three-dimensional (3-D) framework structures could lead to high electrochemical activity and the enhancement of the electrochemical property for supercapacitors [24].
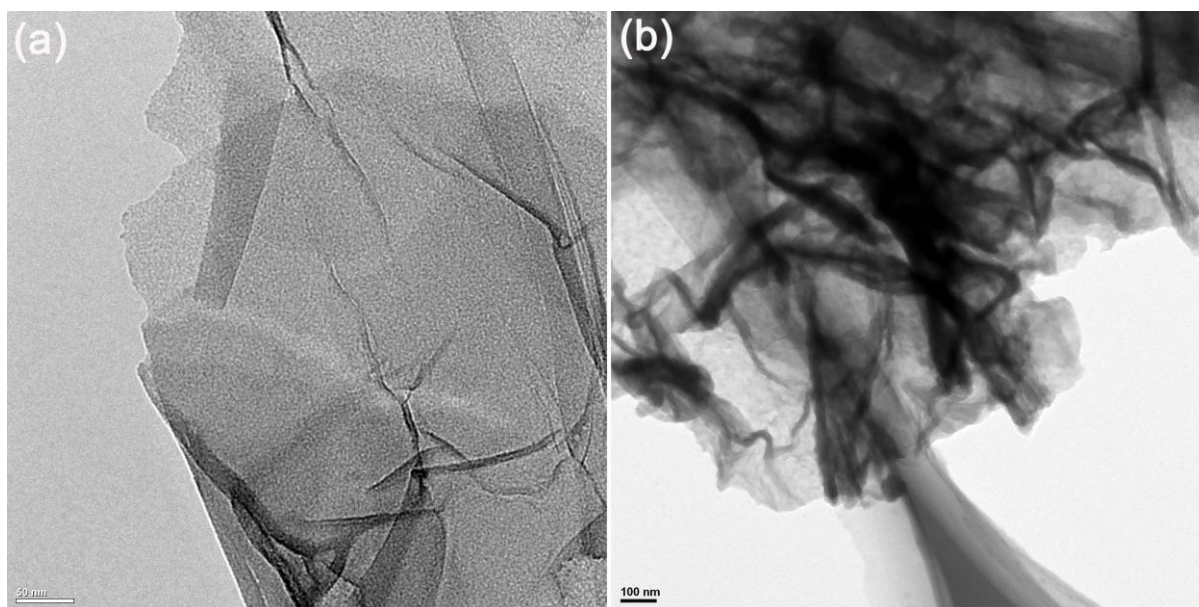

Figure 4. TEM images of (a) GNS and (b) GP_1.

Fig. 4 shows TEM images of GNS and GP_1. The GNS exhibit sheet structures with a lot of wrinks and scrolled, which is like crumpled paper, as shown in Fig. 4a. The image of GP_1 (Fig. 4b) demonstrates that the GNS has been homogeneously surrounded by GNS.

Here we would like to propose the formation mechanism of GNS/PANI composite as shown in Fig. 5. When aniline monomers are added to the GNS suspension, aniline monomers can immediately absorb on the surfaces of GNS due to the electrostatic attraction. It is considered that the degree of electron delocalization was promoted in highly conjugated π-systems between PANI and GNS，leading to preferential protonation of the amine nitrogen atoms [25]. The uniform and tightly stacked PANI layers were formed on the surface of GNS at low contet, resulting in the three-dimensional (3-D) framework structures. When the aniline content increased, the redundant aniline appeared to aggregate while the interaction force between GNS and the PANI layers was weakened, which deteriorated the framework of GNS.
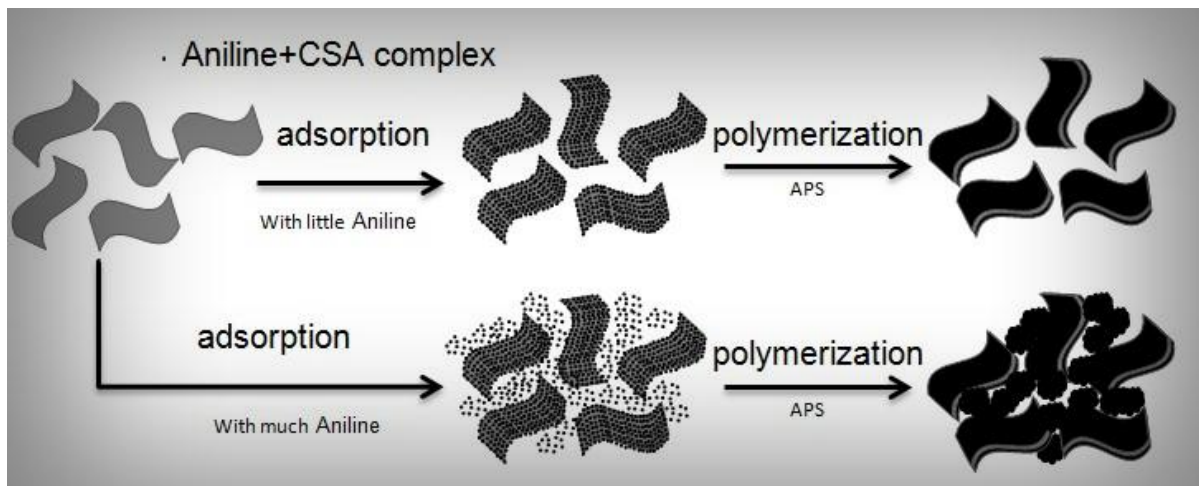
Figure 5. Schematic illustration for the formation mechanism of GNS/PANI composite.
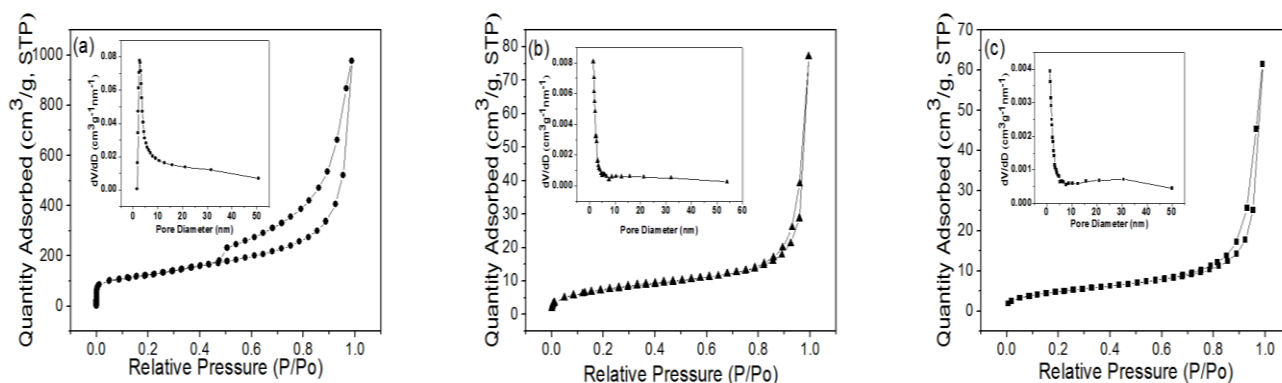

Figure 6. Nitrogen adsorption/desorption isotherms of (a) GNS, (b) GP_1 and (c) GP_2, the inset shows the porosity distribution.

Fig. 6 displays the nitrogen adsorption–desorption isotherms. The specific surface area of GNS was calculated to be 430.8 m^2/g by BET method, whereas the value of GP_1 and GP_2 is 27.5 and 17.9 m^2/g, respectively. The remarkable decrease of specific surface area for the GNS/PANI composite is partially attributed to the disappearance of micropore during the process of surface coating [26]. And the higher BET surface area of GP_1 should be assigned to the undestroyed framework of GNS in the composite. It is obvious that all the samples present the typical IV shapes according to IUPAC classification [27], indicating the mesoporous characteristics. According to the pore size distribution curves, the pore volume of GP_1 is bigger than that of GP_2.

Fig. 7 presents the CV curves of GNS, GP_1 and GP_2 at the scan rate of 10 mV/s in 6 M KOH solution. The supercapacitors based on GNS exhibited an approximately rectangular shape, implying its capacitance is mainly attributed to electric double layer capacitance. In the case of GNS/PANI composite, there is a couple of redox peaks in CV curve, attributed to the redox transition of PANI between a semiconducting state (leucoemeraldine form) and a conducting state (polaronic emeraldine form) [18, 25], leading to the redox capacitance. It can be apparently seen that the surrounded area by

CV curves of GNS/PANI composite is apparently larger than that of pure GNS, indicating the higher specific capacitance. GNS in the composite can offer highly conductive path and serve as a high surface area backbone for the polymerization of PANI, facilitating rapid transport of the electrolyte ions into the electrode during rapid charge/discharge process [28]. Besides, it is found that the redox current increased when scan rate was improved, suggesting the good rate capability. Furthermore, the quasi-rectangle area of each CV curve of GP_1 was larger than that of GP_2, suggesting a larger capacitance than that of the latter.
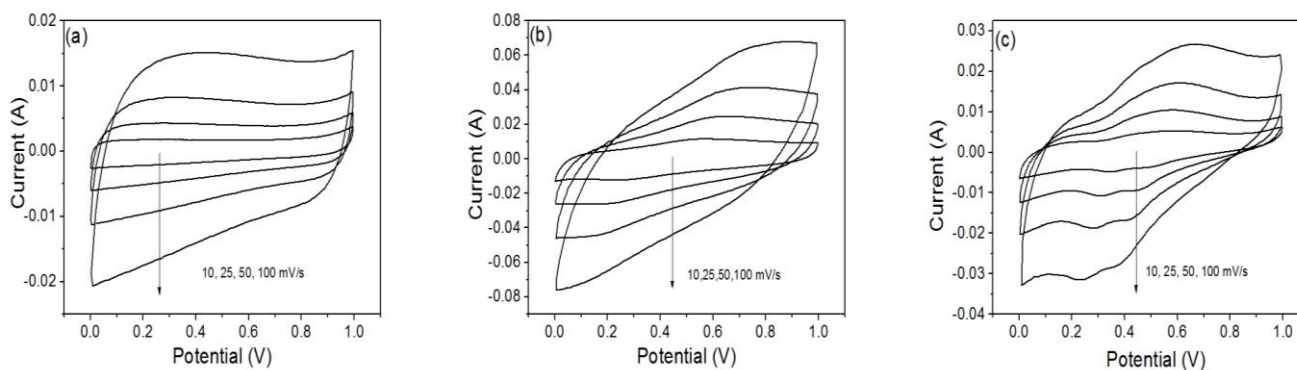

Figure 7. Cyclic voltammograms obtained from (a) GNS, (b) GP_1 and (c) GP_2 electrode at different sweep rates.

The specific capacitance is calculated according to the slope of the charge-discharge curves. The specific capacitance of the electrode is calculated according to the following equation [27]:

$$C_T = \frac{I \times \Delta t}{\Delta V} \qquad (1)$$

$$\frac{1}{C_T} = \frac{1}{m_1 C_s} + \frac{1}{m_2 C_s} \qquad (2)$$

C_T is the total series capacitance of the two electrodes in electrochemical capacitor cell (F), I is the current (A), Δt is the discharging time (s), ΔV is the voltage difference of discharge (V), C_s is the specific capacitance of a single electrode (F/g), m_1 and m_2 are the active mass of the two electrodes, respectively.

Fig. 8(a) demonstrates the relationship of the specific capacitance of the electrode materials and current density. It can be observed that the specific capacitance of GP_1 is much higher than that of GNS and GP_2 at the same current density. The maximum specific capacitance of 261.4 F/g is obtained at the current density of 100 mA/g for GP_1, which is higher than previous reports (233 F/g) [29]. The corresponding data was 190.6 F/g for GNS and 52.8 F/g for GP_2, respectively. For GP_1, the specific capacitance decreased to 180.4 F/g when the current density is up to 1000 mA/g in comparison to

148.9 F/g for GNS. The enhanced specific capacitance and excellent rate capability for GNS/PANI composite is ascribed to the synergetic effect of GNS and PANI. Notably, the GP_2 composite shows the lowest capacitance among all the samples. Because the utilization of GNS is crucial in the realization of pseudocapacitance, its destroyed framework may slow down the charge transport to the underlayer of the GNS.
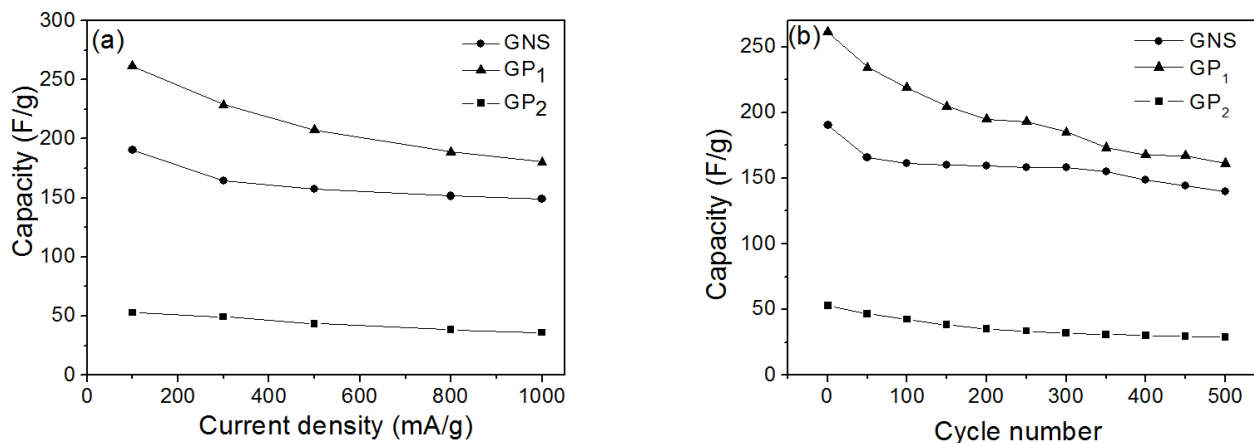

Figure 8. (a) Specific capacitance of GNS, GP_1 and GP_2 at different current density from 0.1 to 1.0 A/g in 6 M KOH solution; (b) Cycling performance of GNS, GP_1 and GP_2 under a current density of 0.1 A/g in 6 M KOH solution.

Fig. 8(b) displays the capacitance versus cycle number for all the three samples at 0.1 A/g current density. The capacitance of the GNS quickly decreased to 139.8 F/g after 500 charge/discharge cycles However, on the same conditions, the capacitance of GP_1 was 161.2 F/g. This demonstrates that the GNS/PANI composite perform better stability than GNS in cycles.

4. CONCLUSIONS

In summary, PANI were successfully coated on the surface of GNS with three-dimensional (3-D) framework structure by using an in-situ polymerization. The synergetic effect of GNS and PANI facilitate the charge-transfer reactions. The electrochemical results show that the undestroyed framework of GNS plays a critical role in the electrochemical performance of the composite. The highest specific capacitance for the composite was observed to be 261.4 F/g at the current density of 100 mA/g in comparision with 190.6 F/g for bare GNS. Such composite with the three-dimensional (3-D) framework structures have been demonstrated to be excellent candidate electrode materials for high-performance supercapacitors.

References

1. B. E. Conway, *Electrochemical Supercapacitors: Scientific Fundamentals and Technological Applications*, Plenum Publishers, New York (1999).
2. K. S. Novoselov, A. K. Geim, S. V. Morozov, D. Jiang, Y. Zhang, S. V. Dubonos, I. V. Grigorieva and A. A. Firsov, *Science*, 306 (2004) 666.
3. M. D. Stoller, S. Park, Y. Zhu, J. An and R. S. Ruoff, *Nano Lett.*, 8 (2008) 3498.
4. S. Vivekchand, C. Rout, K. Subrahmanyam, A. Govindaraj and C. Rao, *Journal of Chemical Sciences*, 120 (2008) 9.
5. J. L. Xia, F. Chen, J. H. Li and N. J. Tao, *Nature Nanotechnology*, 4 (2009) 505.
6. S. Stankovich, D. A. Dikin, G. H. B. Dommett, K. M. Kohlhaas, E. J. Zimney, E. A. Stach, R. D. Piner, S. T. Nguyen and R. S. Ruoff, *Nature*, 442 (2006) 282.
7. J. Yan, T. Wei, B. Shao, F. Ma, Z. Fan, M. Zhang, C. Zheng, Y. Shang, W. Qian and F. Wei, *Carbon*, 48 (2010) 1731.
8. G. X. Wang, B. Wang, X. L. Wang, J. Park, S. X. Dou, H. Ahn and K. Kim, *J. Mater. Chem.*, 19 (2009) 8378.
9. Z.-S. Wu, W. Ren, L. Wen, L. Gao, J. Zhao, Z. Chen, G. Zhou, F. Li and H.-M. Cheng, *Acs Nano*, 4 (2010) 3187.
10. Z. Fan, J. Yan, L. Zhi, Q. Zhang, T. Wei, J. Feng, M. Zhang, W. Qian and F. Wei, *Adv. Mater.*, 22 (2010) 3723.
11. Z. Lei, N. Christov and X. S. Zhao, *Energy & Environmental Science*, 4 (2011) 1866.
12. Q. Wu, Y. Xu, Z. Yao, A. Liu and G. Shi, *Acs Nano*, 4 (2010) 1963.
13. K. Zhang, L. L. Zhang, X. S. Zhao and J. Wu, *Chem. Mater.*, 22 (2010) 1392.
14. H. Wang, Q. Hao, X. Yang, L. Lu and X. Wang, *Electrochem. Commun.*, 11 (2009) 1158.
15. W. S. Hummers and R. E. Offeman, *J. Am. Chem. Soc.*, 80 (1958) 1339.
16. Xinlu Li, Hongfang Song, Hao Wang, Hongyi Li, Y. Zhang and J. Huang, *J. New Mater. Electrochem. Syst.*, 15 (2012) 097.
17. Y. Yan, Q. Cheng, G. Wang and C. Li, J. Power Sources, 196 (2011) 7835.
18. H.-Q. Wang, Z.-S. Li, Y.-G. Huang, Q.-Y. Li and X.-Y. Wang, *J. Mater. Chem.*, 20 (2010) 3883.
19. J. Yan, T. Wei, B. Shao, Z. Fan, W. Qian, M. Zhang and F. Wei, *Carbon*, 48 (2010) 487.
20. Y. Zhu, S. Murali, M. D. Stoller, A. Velamakanni, R. D. Piner and R. S. Ruoff, *Carbon*, 48 (2010) 2118.
21. Y. G. Wang, H. Q. Li and Y. Y. Xia, *Adv. Mater.*, 18 (2006) 2619.
22. Y. Yan, Q. Cheng, G. Wang and C. Li, *J. Power Sources*, 196 (2011) 7835.
23. Y. Zhou, Z.-Y. Qin, L. Li, Y. Zhang, Y.-L. Wei, L.-F. Wang and M.-F. Zhu, *Electrochim. Acta*, 55 (2010) 3904.
24. RamanathanT, A. A. Abdala, StankovichS, D. A. Dikin, M. Herrera Alonso, R. D. Piner, D. H. Adamson, H. C. Schniepp, ChenX, R. S. Ruoff, S. T. Nguyen, I. A. Aksay, R. K. Prud'Homme and L. C. Brinson, *Nat Nano*, 3 (2008) 327.
25. J. Rouquerol, D. Avnir, C. W. Fairbridge, D. H. Everett, J. M. Haynes, N. Pernicone, J. D. F. Ramsay, K. S. W. Sing and K. K. Unger, *Pure Appl. Chem.*, 66 (1994) 1739.
26. J. Zhang and X. S. Zhao, *The Journal of Physical Chemistry C*, 116 (2012) 5420.
27. J. Li, H. Xie, Y. Li, J. Liu and Z. Li, *J. Power Sources*, 196 (2011) 10775.
28. Q.-Y. Li, H.-Q. Wang, Q.-F. Dai, J.-H. Yang and Y.-L. Zhong, *Solid State Ionics*, 179 (2008) 269.
29. D.-W. Wang, F. Li, J. Zhao, W. Ren, Z.-G. Chen, J. Tan, Z.-S. Wu, I. Gentle, G. Q. Lu and H.-M. Cheng, *Acs Nano*, 3 (2009) 1745